

Physical properties and gas hydrate at a near-seafloor thrust fault, Hikurangi Margin, New Zealand

Ann E. Cook¹, Matteo Paganoni², M. Ben Clennell³, David D. McNamara⁴, Michael Nole⁵,
Xiujuan Wang⁶, Shuoshuo Han⁷, Rebecca E. Bell⁸, Evan A. Solomon⁹, Demian M. Saffer⁷,
Philip M. Barnes¹⁰, Ingo A. Pecher¹¹, Laura M. Wallace¹², Leah J. LeVay¹³ & Katerina E.
Petronotis¹³

¹School of Earth Sciences, The Ohio State University, Columbus, Ohio, USA; Corresponding
author: cook.1129@osu.edu

²Department of Earth Sciences, University of Oxford, Oxford, UK & Shell International Global
Solutions, Rijswijk, The Netherlands

³CSIRO, Kensington, Western Australia, Australia

⁴Earth, Ocean and Ecological Sciences, University of Liverpool, Liverpool, UK

⁵Center for Energy and Earth Systems, Sandia National Laboratories, Albuquerque, New
Mexico, USA

⁶Institute of Oceanography, Chinese Academy of Sciences, Quidao, China

⁷Institute for Geophysics, University of Texas-Austin, Austin, Texas, USA

⁸Basins Research Group, Imperial College London, Kensington, UK.

⁹School of Oceanography, University of Washington, Seattle, Washington, USA

¹⁰National Institute of Water and Atmospheric Research (NIWA), Wellington, New Zealand

¹¹School of Environmental and Marine Sciences, University of Auckland, Auckland, New
Zealand

¹²GNS Science, Lower Hutt, New Zealand

¹³International Ocean Discovery Program, Texas A&M University, College Station, Texas, USA

24
25
26
27
28
29
30
31
32
33
34
35
36
37
38
39
40
41
42
43
44
45
46

Key Points

The Pāpaku fault zone is a 33-m thick near-seafloor splay fault drilled at Site U1518 on the Hikurangi Margin. Multiple lines of observational, geophysical and geochemical evidence suggest that there is little to no fluid flow along the Pāpaku fault

Abstract

The Pāpaku fault zone, drilled at IODP Site U1518, is an active splay fault in the frontal accretionary wedge of the Hikurangi Margin. In logging-while-drilling data, the 33 m-thick fault zone exhibits mixed modes of deformation associated with a trend of downward decreasing density, P-wave velocity and resistivity. Methane hydrate are observed from ~30-585 mbsf, including within and surrounding the fault zone. Hydrate accumulations are vertically discontinuous and occur throughout the entire logged section at low to moderate saturation in silty and sandy cm-thick layers. We argue that the hydrate distribution implies that the methane is not sourced from fluid flow along the fault but instead by local diffusion. This, combined with geophysical observations and geochemical measurements from Site U1518, suggests that the fault is not a focused migration pathway for deeply-sourced fluids and that the near-seafloor Pāpaku fault zone has little to no active fluid flow.

Plain Language Summary

Faults are boundaries in the Earth where two different blocks of sediment or rock slide past each other. Offshore New Zealand, the Pāpaku Fault is very shallow and intersects the seafloor but connects to deeper faults kilometers below the seafloor where large earthquakes can occur. An ice-like form of methane called hydrate also occurs within and surrounding the fault. We use scientific drilling data to understand the physical properties of the fault. Hydrate can affect fault properties and how fluid flows; however, based on the pattern of hydrate distribution and other geochemical and geophysical measurements we suggest that the Pāpaku fault does not have active fluid flow.

Keywords: Hikurangi Margin, fault, gas hydrate, accretionary wedge

1. Introduction

The physical and hydrological properties of subduction zone thrust faults are of great interest because of their relationship with large earthquakes. Movement along these faults span a range of behaviors from large earthquakes, to slow and low frequency earthquakes, to aseismic creep behavior [Hyndman *et al.*, 1997; Rogers and Dragert, 2003]. A number of variables influence this spectrum of slip behavior, such as temperature, frictional properties, effective stress and pore pressure [Beroza and Ide, 2011; Saffer and Wallace, 2015; Bürgmann, 2018]. In addition, fault slip behavior near the trench of subduction zones is critical to understand as these areas can generate large tsunamis [Ide *et al.*, 2011]. The fluid flow and drainage patterns of active faults play an important role in mediating the distribution of fluid pressure and effective

stress. These flow patterns are also a first-order control on seepage, dewatering processes, and volatile fluxes in subduction forearcs [e.g. *Moore and Vrolijk*, 1992; *Carson and Screaton*, 1998; *Saffer and Tobin*, 2011].

At the Hikurangi Margin along the eastern North Island of New Zealand, the Pacific plate subducts westward beneath the Australian plate at a rate of ~35-55 mm/year. A range of fault slip styles have been observed or inferred along the Hikurangi Margin including short-term and long-term slow-slip events (SSE), earthquakes, and tsunami earthquakes [*Doser and Webb*, 2003; *Wallace et al.*, 2009, 2012]. Moreover, SSEs at the northern Hikurangi Margin have been observed within 2 km of the seafloor, and these are among the shallowest SSE observations on Earth [*Wallace et al.*, 2016]. The variety of slip styles on the Hikurangi Margin, opportunities for near-field monitoring of SSEs near the trench, and the accessibility of the SSE source to scientific ocean drilling and seismic imaging, makes the area an excellent location to study fault structure, fault properties and fluid flow.

The Pāpaku fault (Figure 1), drilled at International Ocean Discovery Program (IODP) Site U1518, intersects the seafloor in a highly active part of the outer margin. The fault is part of a splay system in the accretionary wedge that connects to the deep décollement 10-25 km landward of the drill site, and 2-3 km deeper [*Barker et al.*, 2018]. While the Pāpaku fault zone has been penetrated at very shallow depths at the drilling location (~315 meters below seafloor, mbsf) it may slip and may exhibit pore pressure and fluid flow changes as a result of SSEs.

An extensive suite of *in situ* measurements were collected across the Pāpaku fault in Hole U1518B using logging-while-drilling (LWD) tools during IODP Expedition 372 (Figure 1) [*Saffer et al.*, 2019b]. About 50 m to the south, the Pāpaku fault was cored at Hole U1518F during Expedition 375 (Figure 1). There was 43% core recovery over a ~300 m interval

surrounding the fault [Saffer et al., 2019b] and 33% recovery in the fault zone [Fagereng et al., 2019]. While this core recovery is comparable to other fault zones, coring alone leaves significant gaps in the characterization of the Pāpaku fault zone and surrounding sedimentary system that can be resolved with continuous LWD measurements.

Methane hydrate, a solid clathrate of methane and H₂O [Sloan and Koh, 2007] was observed in core at Site U1518 at several different intervals from 33-391 mbsf using infrared scanning and pore water chlorinity measurements [Saffer et al., 2019b]. Methane hydrate is stable throughout Site U1518; the top of methane hydrate stability occurs at ~600 m below sea level in the water column (water depth is ~2630 m) and the base of the methane hydrate stability occurs at ~585 mbsf, using the CSMHyd software [Sloan and Koh, 2007] which incorporates measured temperature, background pore water salinity, and estimated pressure [Saffer et al., 2019b]. Hydrate can affect fluid flow patterns by influencing sediment permeability and pore pressure [Nimblett and Ruppel, 2003; Xu and Germanovich, 2006; Sultan, 2007; Daigle et al., 2015] as well as alter the sediment physical properties such as increasing stiffness, cohesion and shear strength [Pearson et al., 1983; Yun et al., 2005; Waite et al., 2009; Yoneda et al., 2017].

The Pāpaku fault now hosts a borehole observatory installed in Hole U1518H (only a few meters from Hole U1518B) that is monitoring pore fluid pressure, fluid flow rates and temperature, as well as sampling fluids for geochemical analyses [Saffer et al., 2019b]. Therefore, the logging and coring datasets collected at Site U1518 yield insight into the properties of the Pāpaku fault, surrounding sediment, hydrate distribution, and the fluid flow system that provides valuable context for the interpretation of fault slip processes and the observatory data [e.g. Sawyer et al., 2008; Kinoshita et al., 2018]. Herein, we interpret LWD

measurements from Hole U1518B and use the distribution of hydrate to infer fluid flow within and around the Pāpaku fault zone.

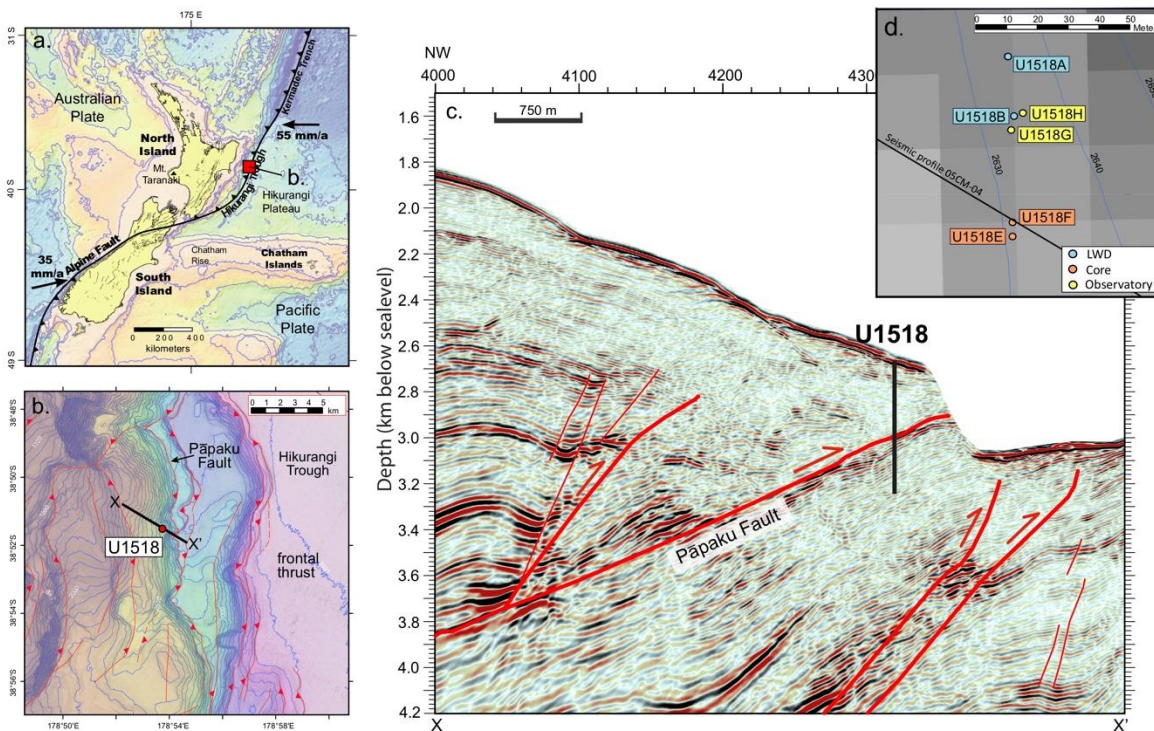


Figure 1. a) Location of Site U1518 offshore the North Island of New Zealand on the Hikurangi Margin. b) Zoomed in bathymetry near the Pāpaku Fault. c) Seismic cross section over the area, with ancillary faults and the Pāpaku Fault identified with red lines. Seismic line location shown in b (black line). d) The placement of six holes at Site U1518. All images are modified from Saffer *et al.*, [2019a; 2019b]. LWD = logging while drilling.

2. Methods

A comprehensive set of *in situ* LWD measurements were collected across the Pāpaku fault in Hole U1518B, which included natural gamma ray, ultrasonic caliper, neutron porosity, source-less neutron density, button, ring and propagation resistivity measurements, resistivity

imaging, P-wave and S-wave velocity, nuclear magnetic resonance (NMR) porosity and NMR T₂ relaxation time distribution [Wallace *et al.*, 2019]. Figure 2 depicts selected measurements across the fault zone from Hole 1518B.

We used Schlumberger's petrophysical analysis software, Techlog, to orient and interpret statically and dynamically normalized resistivity images to identify bedding, fault and fractures orientations [e.g. Wallace *et al.*, 2019]. We also interpreted deformation features in the image, which we define as either non-throughgoing sinusoids fragmented due to deformation, or throughgoing features that change orientation on the image (for example, features appear squeezed and a symmetric sinusoid cannot be fit to the feature), which indicate possible soft-sediment deformation.

We adapt Archie's equation [Archie, 1942] to calculate hydrate saturation, S_h , which is applicable when hydrate is in the primary pore space of water wet sands and silts [Spangenberg, 2001; Goldberg *et al.*, 2010; Priegnitz *et al.*, 2015; Cook and Waite, 2018]. We use RING resistivity, R_{RING} , and an estimated background resistivity, R_o , to calculate S_h :

$$S_h = 1 - \left(\frac{R_o}{R_{RING}} \right)^{1/n} \quad \text{Equation 1}$$

We estimate R_o by carefully considering the background trends in resistivity, P-wave velocity, neutron porosity and NMR porosity; we also conservatively overestimated R_o in intervals with borehole washout. R_{RING} is used in saturation calculations because it is the most sensitive resistivity measurement for hydrate in cm-thick layers due to the high vertical resolution (5-8 cm) for depth of penetration [Cook *et al.*, 2012]. For the saturation exponent, n , we apply $n = 2$ & $n = 3$ to show the probable range of hydrate saturations [Cook and Waite, 2018]. We also

calculated R_o from neutron porosity for comparison, but we did not use it for saturation calculations (see Supporting Information).

Other than hydrate, sediment overcompaction or cementation could cause spikes in resistivity, but 1) cements are not observed in the core at Site U1518 [Saffer *et al.*, 2019b] and 2) there is no decrease in neutron porosity or NMR porosity indicating cementation or overcompaction at the locations of any of the thicker resistivity spikes; thus hydrate the most likely cause of resistivity exceeding R_o throughout Site U1518.

3. The Pāpaku fault zone & surrounding system

In the LWD data, we observe significant changes in the physical properties and bedding orientation above, below and within the Pāpaku fault zone (Figure 2), which are described in the following section. Overall, more deformation features are identified in the hanging wall (Figure 2), which may explain the acoustic transparency in the hanging wall relative to the footwall on seismic data (Figure 1c).

On the LWD data, we observe hydrate concentrated in thin layers (on the order of cm to 10's of cm) above, below and within the Pāpaku fault zone (Figure 2). Centimeter to tens of cm-thick coarse-grained (sand and silt) layers were observed throughout Site U1518 in cores [Saffer *et al.*, 2019b]. We identify these coarse-grained layers on LWD data by local gamma ray lows, and note that almost all layers with $S_h > 0.2$ is associated with a local gamma ray low (Figure 2). While there is variation in hydrate concentrations with depth, there is not a large difference in the concentration of hydrate filled layers in the hangingwall, fault zone and footwall (Figure 2). Some of the variation may be due to the occurrence of coarse-grained layers. The fault zone itself does

have lower hydrate saturations (<0.1) than the immediate surrounding hanging wall and footwall, however, other sections such as 235-263 mbsf in the hanging wall and 455-485 mbsf in the footwall also have similar low hydrate saturations (<0.1).

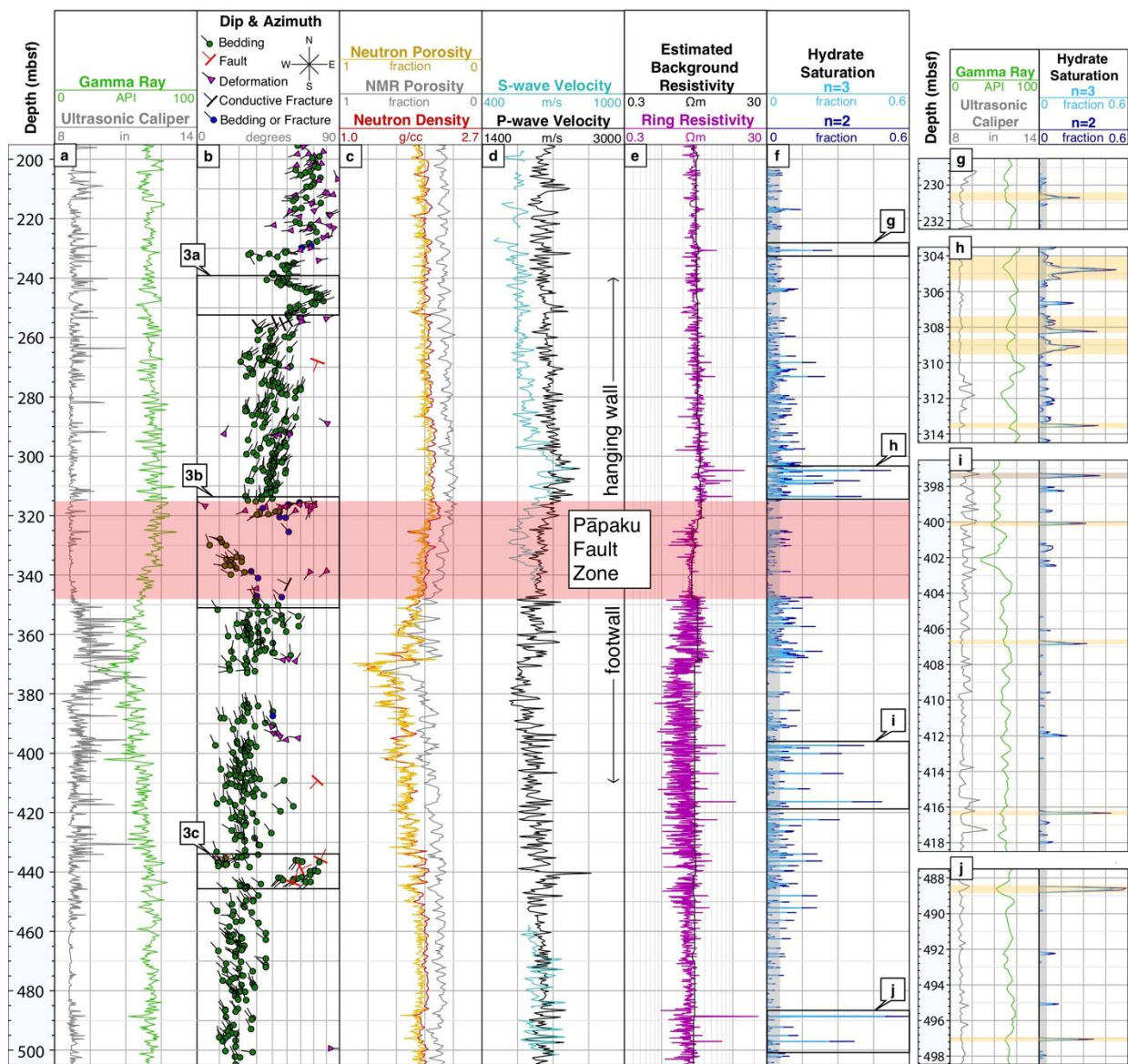


Figure 2. a. Logging-while-drilling (LWD) well log measurements (Tracks a, c, d & e), image interpretation (Track b), estimated background resistivity (Track e) and calculated hydrate saturation (Track f) at Hole U1518B. Note that the neutron porosity and neutron density may not provide accurate measurements in this high porosity, clay rich environment, and NMR porosity measurements are affected by the presence of gas hydrate. When resistivity is low and close to the background, calculated hydrate saturations (Track f) have lower confidence; we grayed these lower confidence saturations. At low resistivity, intervals without hydrate could be identified with low saturation and intervals could be incorrectly identified as water-saturated. Insets g, h, i

and j show enlarged intervals in U1518B in thin layers. All layers greater than ~20% that are associated with gamma ray lows are highlighted in yellow on the insets (10 layers); one layer that was not associated with a gamma ray low was highlighted in brown on Inset i.

3.1 Hanging wall and fault zone

In core from Hole U1518F, the Pāpaku fault zone was identified from 304-361 mbsf, which includes an ~18 m-thick fault zone underlain by ~30 m of less deformed material, followed by a ~10 m-thick subsidiary fault zone [Fagereng *et al.*, 2019]. The Pāpaku fault zone depths are different in LWD Hole U1518B ~50 m to the north, where we interpret the base of the hanging wall and the top of the Pāpaku fault zone to begin 11 meters deeper, at 315 mbsf, where there is an abrupt change from 25-45° north-dipping beds to a chaotically oriented and deformed interval (Figure 3b) [Fagereng *et al.*, 2019; Saffer *et al.*, 2019].

The base of the hanging wall (300-315 mbsf) is marked by elevated P-wave and S-wave velocity and low neutron porosity. Increased compaction and shear strengthening from fault movement compared to the adjacent intervals may explain such trends. However, this interval also hosts hydrate (Figure 2b), which contributes to the increase in P-wave and S-wave velocity by increasing the cohesive and mechanical strength. The hydrate is occurring at saturations up to 0.5 in 10's of cm-thick layers that are generally coarser-grained (Figure 2h).

The bedding orientation from the hanging wall (dipping 25-45° north) is truncated against chaotically dipping features which are a combination of deformation, fractures and bedding (Figure 3b). The interval between 315-321 mbsf has the highest density values in the hole, likely related to increased compaction caused by fault movement, though the P-wave and S-wave velocity are lower than the interval just above that contains hydrate (Figure 2).

Most of the fault zone in Hole U1518B is marked by a gradual decrease in P-wave velocity, resistivity and neutron density with depth. These LWD measurements are of high quality in the fault zone as the borehole diameter is close to the bit size, however, bedding and fracture orientation is often difficult to distinguish within the fault zone as the image appears mottled (Figures 2 & 3). A variety of deformation features were observed in the core, including breccia, flow banding, breccia clasts, dismembered beds, small faults and fractures [Fagereng et al., 2019]. The mottled appearance observed on the image logs over several large sections in the fault zone (Figure 3b) are likely caused by discontinuous deformation features smaller than several horizontal image bins (~3-5 cm) and the vertical resolution (~5-8 cm) of the resistivity images [Luthi, 2001; Schlumberger, 2007]. Bright white mottled features on the image log (Figure 3b) may also be hydrate forming in nodules or in deformed coarser-grained layers within the fault zone. Intervals in the fault zone with identified bedding may be a relatively intact section within the fault zone or could be deformed beds or flow banding.

Below ~335 mbsf, the gamma ray (Figure 2) and NMR T2 distribution (shown in [Saffer et al., 2019b]) indicate sediment gradually grades into a nearly 100 m-thick, coarse-grained unit of silts and sands with thin mud interbeds; the bottom of the fault zone is near the top of this coarse-grained unit at 340-348 mbsf.

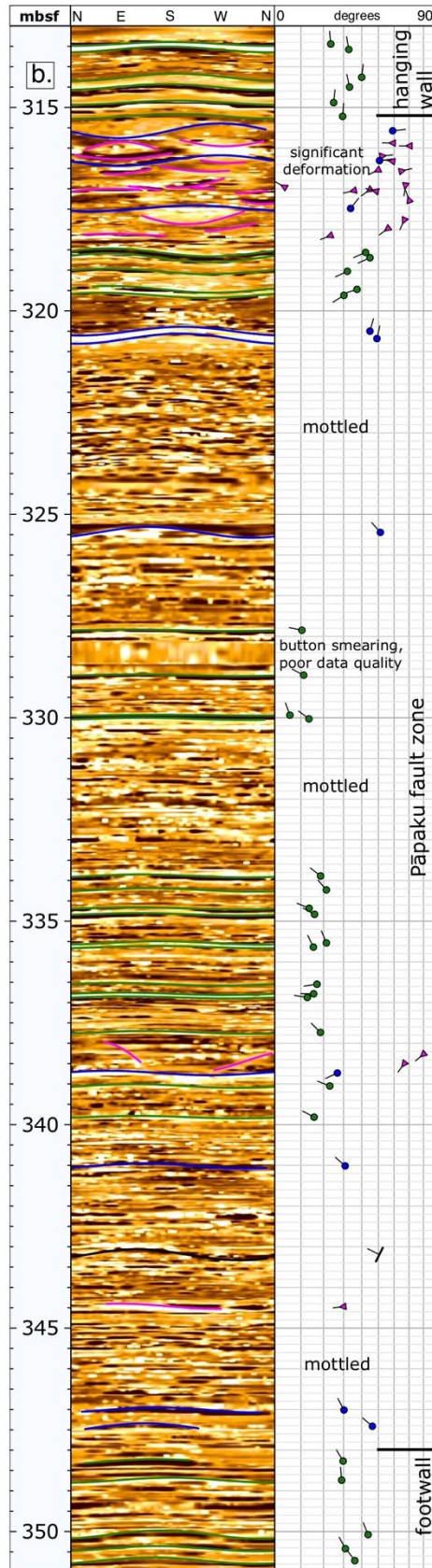
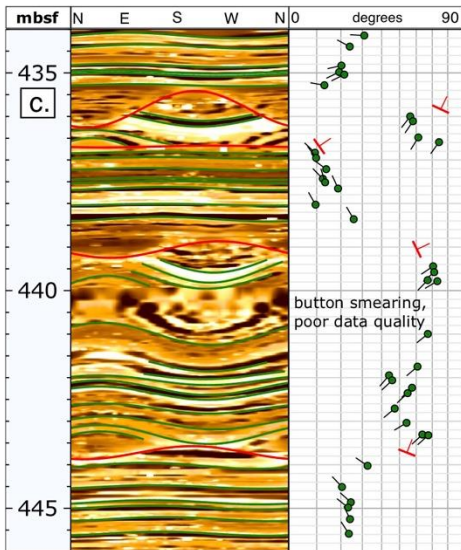
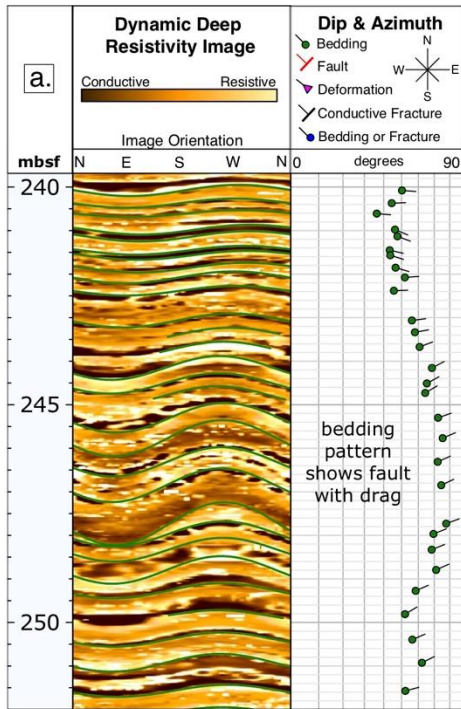


Figure 3. Selected resistivity image log intervals and interpretation from Hole U1518B. a) Bedding patterns indicating a thrust fault propagation fold, b) the Pāpaku fault zone and c) a section of faults and offset beds in the footwall. Higher resolution image logs and interpretation are available in Supporting Information (Figure S1).

3.2 Footwall

The base of the Pāpaku fault zone and the transition to the footwall is not as clear as the hanging wall transition on LWD data. Part of this ambiguity is due to the lithology, as grading into coarser sediments is indicated by the gamma ray beginning at ~335 mbsf, making it difficult to distinguish between physical property changes from coarsening sediment versus changes produced by deformation processes within the fault zone. Core observations note silts and hemipelagic mud at the bottom the fault zone and the top of the footwall, however, core recovery was low in the footwall (<36%) which may be due to coarser-grained sands and silts being washed out during drilling [Saffer *et al.*, 2019b].

We argue the most likely depth for the base of the Pāpaku fault zone on LWD data is 340-348 mbsf. At this depth, there are only a few features identified on the image logs (Figure 3), suggesting the interval may still be affected by fault-related deformation. The contrasting bedding orientations above 340 and below 348 mbsf further suggests there is deformation occurring in this interval. Below 348 mbsf, most identified beds have a similar orientation to beds significantly below the fault zone (i.e. from ~450-500 mbsf) indicating that this is the footwall.

3.3 Subsidiary faults

There are several subsidiary faults and fault-related features visible on the LWD resistivity images. Six faults identified at 272, 409, 436, 437, 439, and 444 mbsf are dipping between 12-75° (Figure 2). Figure 3c shows four of these faults, which occur between 435-445 mbsf and are associated with sharp changes in bedding orientation above and below the fault sinusoid. We cannot identify the relative movement of these faults because beds cannot be correlated above and below the fault plane sinusoid. This also means that the throw is more than the amplitude of the sinusoid in the borehole (between 10-100 cm).

A major fault zone was interpreted at 351-361 mbsf in coring Hole U1518F [*Fagereng et al.*, 2019] and at 369 mbsf in LWD Hole U1518B [*Saffer et al.*, 2019b]. LWD evidence for a fault near 369 mbsf includes changing bedding orientations from 368-370 mbsf with some deformation features; however, there is no clear fault plane like other subsidiary faults observed in the resistivity images (Figure 3c). In addition, there are several depths (e.g. 226, 234, and 355 mbsf) where bedding orientation changes suddenly which could also be evidence for additional faults.

Another fault-related feature is the orientation of beds from 242-250 mbsf (Figure 3a), which increase in dip from 242 mbsf and reach the highest angle dip of almost 80° at ~247 mbsf and then decreases. This pattern of increasing and decreasing dip is consistent with a thrust fault-propagation fold as well as the stress regime in the hanging wall.

4 Discussion

On LWD data from Hole U1518B, we interpret an apparent 33 m-thick Pāpaku fault zone from 315-348 mbsf. From core in Hole U1518F, *Fagereng et al.* [2019] interpreted the fault

zone over an apparent 58 m-thick interval from 304-361 mbsf. The top of the fault zone is identified in both LWD and core datasets by a low porosity interval at the base of the hanging wall and at the top of the fault zone [Saffer *et al.*, 2019a]. The difference in the Pāpaku fault zone thickness and the top of the fault zone may be the result of a variety of different factors [Saffer *et al.*, 2019b]. There may be a change in fault geometry and thickness over the 50 m distance between holes due to splays or imbricate structure, or poor core recovery may cause an overestimate of fault thickness in the coring hole. Small differences in fault thickness may also be related to borehole deviation.

4.1 Fluid flow and gas hydrate

Hydrate is inferred in many thin, cm- to 10's of cm-thick coarse-grained sediments throughout Site U1518, from as shallow as ~33 mbsf in core samples [Saffer *et al.*, 2019a] to nearly total depth (590 mbsf) on LWD data (Figure 2 & S2). Such a frequent occurrence of hydrate implies that the dissolved pore water methane concentration is very close to solubility throughout the site, yet hydrate appears to preferentially form in higher concentrations in coarse-grained sediments with less hydrate in marine muds.

This pattern of hydrate-bearing coarse-grained layers interbedded within water-saturated or low-hydrate saturation marine muds has been observed in several locations, such as accretionary prisms in the northern Cascadia Margin, the Andaman Sea, and the Nankai Trough as well as in the Gulf of Mexico [Malinverno, 2010; Cook and Malinverno, 2013; Malinverno and Goldberg, 2015]. The pattern can be explained by a diffusion-dominated methane migration, which is driven by the difference in methane solubility between coarse-grained sands (or silts) and marine muds [Malinverno, 2010; Nole *et al.*, 2017; Vanderbeek and Rempel, 2018]. The solubility threshold is

higher in muds due the high curvature of the pore surface in small pores [Clennell *et al.*, 1999; Rempel, 2011]. In marine muds near the seafloor, methane can be generated through a series of microbial reactions, and it is dissolved in the pore water. This methane diffuses into adjacent sand layers over time, and when the solubility threshold is reached, hydrate forms in the sands first. Because methane solubility is lower in the sands, this allows for a diffusive flux of methane dissolved in pore water from marine muds both above and below the sand layers, which can continue to occur as hydrate forms. Eventually, this leads to significant hydrate saturation in thin sands surrounded by water-saturated marine muds. Because the methane generated in the muds only diffuses a few centimeters to meters to fill the thin sands, the mechanism is referred to as short-migration [Malinverno, 2010].

Yet, in accretionary wedge environments advective methane fluxes along faults are observed at many locations worldwide [Moore and Vrolijk, 1992; Kastner *et al.*, 1998, 2014; Geersen *et al.*, 2016] as well as observed and inferred along the Hikurangi Margin, often associated with gas hydrate systems on seismic data [Pecher *et al.*, 2010; Crutchley *et al.*, 2011; Plaza-Faverola *et al.*, 2012; Kroeger *et al.*, 2015; Watson *et al.*, 2019]. In addition, the Pāpaku fault zone at Site U1518 does have relatively high porosity (>0.4) in deformed and fractured sediment which could facilitate fluid flow.

We argue, however, that there is combined observational, geochemical, geophysical and petrophysical evidence supporting little to no advection of deeply-sourced, gas-bearing or geochemically distinct fluids along the Pāpaku fault zone. First, methane to ethane ratios in headspace gas samples are greater than 20,000, suggesting that a microbial origin for the methane is more likely than a deeply-sourced thermogenic origin [Saffer *et al.*, 2019b]. We recognize that

thermogenic methane can be microbially altered and microbial methane can be generated rather deep in some systems and advected upward (for example, modeling suggests microbial generation peaks at 1600 mbsf in the Pegasus Basin in the southern Hikurangi Margin [Kroeger *et al.*, 2015]). Even so, an in-situ microbial origin for the methane forming hydrate appears more in line with the observed pattern of hydrate distribution.

At Site U1518, if the methane originated from fluid or gas flow along the Pāpaku fault one would expect hydrate to occur within and around the fault zone, or perhaps in other large permeable layers like the coarse-grained unit from ~345-440 mbsf. In addition, it is likely that hydrate would form at high-concentration in fractures or veins, as they commonly do in other focused flow settings [Weinberger and Brown, 2006; Abegg *et al.*, 2007; Riedel *et al.*, 2010; Kim *et al.*, 2013]; however, there is no evidence for hydrate in veins or fractures on resistivity images or measurements in Hole U1518B. While we observe an increase in hydrate concentration immediately surrounding the fault zone (Figure 2), the overall saturation is still moderate to low, and we also observe that hydrate occurs throughout the site (from ~30 to 590 mbsf) in thin, discrete layers on the order of cm to 10s of cm-thick. This distribution of hydrate implies that either the fault zone is not the only source of methane or that the fault zone is not related to the methane hydrate distribution.

Other sources of evidence indicate that there is no active fluid flow along the Pāpaku fault. Pore water solute profiles indicated there is no evidence for fluid flow along the fault and the absence of diagenetic cements at Site U1518 further support the lack of fluid advection [Saffer *et al.*, 2019b]. In seismic data, high amplitude, reversed seafloor-polarity reflections from the decollement and other thrust faults on subduction margins have been linked to possible evidence

of fluid flow and/or high pore pressure in both observations and in models [Moore *et al.*, 1995; Bangs *et al.*, 1999, 2015; Saffer and Tobin, 2011]. At the Pāpaku fault, the reverse-seafloor polarity reflection can be produced by the reduction in both P-wave velocity and density from the hanging wall into the fault zone (Figure 2), as shown by the synthetic seismogram in Saffer *et al.*, [2019b]. Therefore, fluid flow and high pore pressure are not required at Site U1518 to explain the negative impedance on seismic data, and the impedance can be explained by changes in physical properties. In addition, a 2D high-resolution full waveform inversion P-wave velocity model by Gray *et al.*, [2019] showed that some fault zones in the wedge are associated with velocity reductions of up to 500 m/s. The smaller velocity reduction of ~100 m/s in the Pāpaku fault zone in the Gray *et al.* [2019] model indicates that the fault may not be acting as a significant conduit for fluid flow in the same way as inferred for other faults.

Collectively, multiple lines of evidence suggest the shallow part of the Pāpaku fault zone currently has low or no fluid advection; however, we cannot rule out fluid flow at greater depths or brief pulses of fluids along the shallow fault zone in the past. If pulsing occurred in the past, the fluids are likely through-going and not interacting with the surrounding footwall and hanging wall system.

Although evidence for long distance migration of fluids is fairly common from drilling frontal thrust faults at subduction zones, another example of a location where there is limited evidence for fluid flow and methane flux is along the Kumano transect on the Nankai Trough [Screaton *et al.*, 2009]. Together, the Kumano and Hikurangi sites suggest that inactive or lower advection hydrologic systems along frontal thrusts could be a more common occurrence than previously thought. How shallow faults without advection may or may not relate to the deeper

fault system is unknown. In the future, data and fluid samples recovered from the borehole observatory installed at Site U1518 will provide direct constraints on in situ near-seafloor fluid flow rates and fault zone hydrologic properties of the Pāpaku fault zone.

5 Conclusions

Understanding physical properties and fluid flow around subduction fault zones is essential for illuminating the role of fluids in fault mechanics and slip behavior. Herein, we argue that the Pāpaku fault zone does not have significant fluid flow in the near-seafloor system. The 33 m-thick fault zone does have high porosity and a trend of decreasing P-wave velocity from top to bottom of the fault. Despite high porosity measured within the fault zone and the occurrence of methane hydrate in thin sands and silts at Site U1518, we argue that advective fluid flow is likely not causing the unconnected but frequent occurrence of gas hydrate from 30 to 585 mbsf on logging-while-drilling (LWD) data. Instead we argue that the hydrate distributed in coarse-grained layers less than 1 m-thick is caused by local diffusion of microbially generated methane. This further supports evidence from geochemical analysis on pore water samples and modeling work on seismic data that the Pāpaku fault does not have significant active fluid flow.

Acknowledgements

This research used data and samples provided by the International Ocean Discovery Program (IODP) and the data in this paper can be accessed through IODP's database

(http://mlp.ldeo.columbia.edu/logdb/scientific_ocean_drilling/). We gratefully acknowledge IODP, Texas A&M university staff, Schlumberger Drilling & Measurements, the crew of the *JR*, and the Expedition 375 and 372 science parties. We thank Schlumberger for the Techlog software donation. We thank A. Malinverno and G. Guerin for their comments and suggestions on this paper.

Cook was supported by NSF Award 1752882, Paganoni was funded by NERC Grant NE/R016615/1 and Bell from NERC Grant NE/S00291X/1, Wang was supported by National Natural Science Foundation of China (41976077), and McNamara was supported by the Geological Survey Ireland. Barnes and Wallace acknowledge support from the New Zealand Endeavour fund, Contract CO5X1605, as well as NIWA and GNS SSIF core funding. LeVay and Petronotis were supported by IODP-JRSO NSF Award 1326927.

-
- Abegg, F., G. Bohrmann, J. Freitag, and W. Kuhs (2007), Fabric of gas hydrate in sediments from Hydrate Ridge - Results from ODP Leg 204 samples, *Geo-Marine Lett.*, 27(2–4), 269–277, doi:10.1007/s00367-007-0080-4.
- Archie, G. E. (1942), The electrical resistivity log as an aid in determining some reservoir characteristics, in *Transactions of the American Institute of Mining and Metallurgical Engineers*, Vol. 146, pp. 54–63.
- Bangs, N. L., K. D. McIntosh, E. A. Silver, J. W. Kluesner, and C. R. Ranero (2015), Fluid accumulation along the Costa Rica subduction thrust and development of the seismogenic zone, *J. Geophys. Res. Solid Earth*, 120, 67–86, doi:10.1002/2014JB011265.
- Bangs, N. L. B., T. H. Shipley, J. C. Moore, and G. F. Moore (1999), Fluid accumulation and channeling along the northern Barbados Ridge Decollement thrust, *J. Geophys. Res. Solid Earth*, 104, 20399–20414, doi:10.1029/1999JB900133.
- Barker, D. H. N., S. Henrys, F. Caratori Tontini, P. M. Barnes, D. Bassett, E. Todd, and L. Wallace (2018), Geophysical Constraints on the Relationship Between Seamount Subduction, Slow Slip, and Tremor at the North Hikurangi Subduction Zone, New Zealand, *Geophys. Res. Lett.*, 45(23), 12,804–12,813, doi:10.1029/2018GL080259.
- Beroza, G. C., and S. Ide (2011), Slow Earthquakes and Nonvolcanic Tremor, *Annu. Rev. Earth Planet. Sci.*, 39(1), 271–296, doi:10.1146/annurev-earth-040809-152531.

- Bürgmann, R. (2018), The geophysics, geology and mechanics of slow fault slip, *Earth Planet. Sci. Lett.*, 495, 112–134, doi:10.1016/j.epsl.2018.04.062.
- Carson, B., and E. J. Screaton (1998), Fluid flow in accretionary prisms: Evidence for focused, time-variable discharge, *Rev. Geophys.*, (36), 329–351, doi:https://doi.org/10.1029/97RG03633.
- Clennell, M. Ben, M. Hovland, S. Booth, H. Pierre, and J. Winters (1999), Formation of Gas Hydrate in Marine Sediments: 1. Conceptual Model of Gas Hydrate Growth Conditioned by Host Sediment Properties, , 104, doi:10.1029/1999JB900175.
- Cook, A. E., and A. Malinverno (2013), Short migration of methane into a gas hydrate-bearing sand layer at Walker Ridge, Gulf of Mexico, *Geochemistry, Geophys. Geosystems*, 14(2), 283–291, doi:10.1002/ggge.20040.
- Cook, A. E., and W. F. Waite (2018), Archie’s Saturation Exponent for Natural Gas Hydrate in Coarse-Grained Reservoirs, *J. Geophys. Res. Solid Earth*, 123(3), doi:10.1002/2017JB015138.
- Cook, A. E., B. I. Anderson, J. Rasmus, K. Sun, Q. Li, T. S. Collett, and D. S. Goldberg (2012), Electrical anisotropy of gas hydrate-bearing sand reservoirs in the Gulf of Mexico, *Mar. Pet. Geol.*, 34(1), doi:10.1016/j.marpetgeo.2011.09.003.
- Crutchley, G. J., A. R. Gorman, I. A. Pecher, S. Toulmin, and S. A. Henrys (2011), Geological controls on focused fluid flow through the gas hydrate stability zone on the southern Hikurangi Margin of New Zealand, evidenced from multi-channel seismic data, *Mar. Pet. Geol.*, 28(10), 1915–1931, doi:10.1016/j.marpetgeo.2010.12.005.
- Daigle, H., A. Cook, and A. Malinverno (2015), Permeability and porosity of hydrate-bearing sediments in the northern Gulf of Mexico, *Mar. Pet. Geol.*, 68, 551–564, doi:10.1016/j.marpetgeo.2015.10.004.
- Doser, D. I., and T. H. Webb (2003), Source parameters of large historical (1917–1961) earthquakes, North Island, New Zealand, *Geophys. J. Int.*, 152(3), 795–832, doi:10.1046/j.1365-246X.2003.01895.x.
- Fagereng, Å., H. M. Savage, J. K. Morgan, M. Wang, F. Meneghini, P. M. Barnes, R. Bell, H. Kitajima, D. D. McNamara, and D. M. Saffer (2019), Mixed deformation styles observed on a shallow subduction thrust, Hikurangi margin, New Zealand, *Geology*, 47(9), 1–5, doi:10.1130/G46367.1/4797825/g46367.pdf.
- Geersen, J., F. Scholz, P. Linke, M. Schmidt, D. Lange, J. Behrmann, D. Volker, and C. Hensen (2016), Fault zone controlled seafloor methane seepage in the rupture area of the 2010 Maule earthquake, Central Chile, *Geochemistry, Geophys. Geosystems*, 17, 4802–4813, doi:10.1002/2015GC006171.Received.
- Goldberg, D. S., R. L. Kleinberg, J. L. Weinberger, A. Malinverno, P. J. McLellan, and T. S. Collett (2010), 16. Evaluation of Natural Gas-Hydrate Systems Using Borehole Logs, *Geophys. Charact. Gas Hydrates*, 239–261, doi:10.1190/1.9781560802197.ch16.
- Gray, M., R. E. Bell, J. V. Morgan, S. Henrys, and D. H. N. Barker (2019), Imaging the Shallow Subsurface Structure of the North Hikurangi Subduction Zone, New Zealand, Using 2-D Full-Waveform Inversion, *J. Geophys. Res. Solid Earth*, 124(8), 9049–9074, doi:10.1029/2019JB017793.
- Hyndman, R. D., M. Yamano, and D. A. Oleskevich (1997), The seismogenic zone of subduction thrust faults, *Isl. Arc*, 6(3), 244–260, doi:10.1111/j.1440-1738.1997.tb00175.x.
- Ide, S., A. Baltay, and G. C. Beroza (2011), Shallow Dynamic Overshoot and Energetic Deep Rupture in the 2011, *Science* (80-.), 332, 1426–1430, doi:10.1126/science.1207020.

- Kastner, M., K. A. Kvenvolden, and T. D. Lorenson (1998), Chemistry, isotopic composition, and origin of a methane-hydrogen sulfide hydrate at the Cascadia subduction zone, *Earth Planet. Sci. Lett.*, 156(3–4), 173–183, doi:10.1016/S0012-821X(98)00013-2.
- Kastner, M., E. A. Solomon, R. N. Harris, and M. E. Torres (2014), Fluid Origins, Thermal Regimes, and Fluid and Solute Fluxes in the Forearc of Subduction Zones, in *Developments in Marine Geology, Volume 7*, pp. 671–733.
- Kim, G. Y., B. Narantsetseg, B. J. Ryu, D. G. Yoo, J. Y. Lee, H. S. Kim, and M. Riedel (2013), Fracture orientation and induced anisotropy of gas hydrate-bearing sediments in seismic chimney-like-structures of the Ulleung Basin, East Sea, *Mar. Pet. Geol.*, 47, 182–194, doi:10.1016/j.marpetgeo.2013.06.001.
- Kinoshita, C. et al. (2018), Changes in Physical Properties of the Nankai Trough Megasplay Fault Induced by Earthquakes, Detected by Continuous Pressure Monitoring, *J. Geophys. Res. Solid Earth*, 123(2), 1072–1088, doi:10.1002/2017JB014924.
- Kroeger, K. F., A. Plaza-Faverola, P. M. Barnes, and I. A. Pecher (2015), Thermal evolution of the New Zealand Hikurangi subduction margin: IMPACT on natural gas generation and methane hydrate formation - A model study, *Mar. Pet. Geol.*, 63, 97–114, doi:10.1016/j.marpetgeo.2015.01.020.
- Luthi, S. (2001), *Geological Well Logs: Their Use in Reservoir Modeling*, Springer-Verlag Berlin Heidelberg.
- Malinverno, A. (2010), Marine gas hydrates in thin sand layers that soak up microbial methane, *Earth Planet. Sci. Lett.*, 292(3–4), 399–408, doi:10.1016/j.epsl.2010.02.008.
- Malinverno, A., and D. S. Goldberg (2015), Testing short-range migration of microbial methane as a hydrate formation mechanism: Results from Andaman Sea and Kumano Basin drill sites and global implications, *Earth Planet. Sci. Lett.*, 422, 105–114, doi:10.1016/j.epsl.2015.04.019.
- Moore, J. C., and P. Vrolijk (1992), Fluids in accretionary prisms, *Rev. Geophys.*, 30(2), 113–135, doi:https://doi.org/10.1029/92RG00201.
- Moore, J. C., G. F. Moore, G. R. Cochran, and H. J. Tobin (1995), Negative-polarity seismic reflections along faults of the Oregon accretionary prism: indicators of overpressuring, *J. Geophys. Res.*, 100(B7), doi:10.1029/94jb02049.
- Nimblett, J., and C. Ruppel (2003), Permeability evolution during the formation of gas hydrates in marine sediments, *J. Geophys. Res. Solid Earth*, 108(B9), 1–17, doi:10.1029/2001jb001650.
- Nole, M., H. Daigle, A. E. Cook, J. I. T. Hillman, and A. Malinverno (2017), Linking basin-scale and pore-scale gas hydrate distribution patterns in diffusion-dominated marine hydrate systems, *Geochemistry, Geophys. Geosystems*, 18, 653–675, doi:10.1002/2016GC006662.
- Pearson, C. F., P. M. Halleck, P. L. McGuire, R. Hermes, and M. Mathews (1983), Natural gas hydrate deposits: a review of in situ properties, *J. Phys. Chem.*, 87(21), 4180–4185, doi:10.1021/j100244a041.
- Pecher, I. A. et al. (2010), Focussed fluid flow on the Hikurangi Margin, New Zealand - Evidence from possible local upwarping of the base of gas hydrate stability, *Mar. Geol.*, 272(1–4), 99–113, doi:10.1016/j.margeo.2009.10.006.
- Plaza-Faverola, A., D. Klaeschen, P. Barnes, I. Pecher, S. Henrys, and J. Mountjoy (2012), Evolution of fluid expulsion and concentrated hydrate zones across the southern Hikurangi subduction margin, New Zealand: An analysis from depth migrated seismic data, *Geochemistry, Geophys. Geosystems*, 13(8), doi:10.1029/2012GC004228.

- Priegnitz, M., J. Thaler, E. Spangenberg, J. M. Schicks, J. Schrötter, and S. Abendroth (2015), Characterizing electrical properties and permeability changes of hydrate bearing sediments using ERT data, *Geophys. J. Int.*, 202(3), 1599–1612, doi:10.1093/gji/ggv245.
- Rempel, A. W. (2011), A model for the diffusive growth of hydrate saturation anomalies in layered sediments, *J. Geophys. Res. Solid Earth*, 116(10), 1–15, doi:10.1029/2011JB008484.
- Riedel, M., T. S. Collett, P. Kumar, A. V. Sathe, and A. Cook (2010), Seismic imaging of a fractured gas hydrate system in the Krishna-Godavari Basin offshore India, *Mar. Pet. Geol.*, 27(7), doi:10.1016/j.marpetgeo.2010.06.002.
- Rogers, G., and H. Dragert (2003), Episodic Tremor and Slip on the Cascadia Subduction Zone, *Science* (80-.), 300, 1942–1944, doi:10.1126/science.1084783.
- Saffer, D. M., and H. J. Tobin (2011), Hydrogeology and Mechanics of Subduction Zone Forearcs: Fluid Flow and Pore Pressure, *Annu. Rev. Earth Planet. Sci.*, 39(1), 157–186, doi:10.1146/annurev-earth-040610-133408.
- Saffer, D. M., and L. M. Wallace (2015), The frictional, hydrologic, metamorphic and thermal habitat of shallow slow earthquakes, *Nat. Geosci.*, 8(8), 594–600, doi:10.1038/ngeo2490.
- Saffer, D. M., L. M. Wallace, P. M. Barnes, I. A. Pecher, K. E. Petronotis, L. J. LeVay, and the E. 372/375 Scientists (2019a), Expedition 372B / 375 summary, *Proc. Int. Ocean Discov. Progr. Vol. 372B/375*, 372B/375, doi:https://doi.org/10.14379/iodp.proc.372B375.101.2019.
- Saffer, D. M. et al. (2019b), Site U1518, *Proc. Int. Ocean Discov. Progr. Vol. 372B/375*, 372B/375.
- Sawyer, A. H., P. Flemings, D. Elsworth, and M. Kinoshita (2008), Response of submarine hydrologic monitoring instruments to formation pressure changes: Theory and application to Nankai advanced CORKs, *J. Geophys. Res. Solid Earth*, 113(1), 1–16, doi:10.1029/2007JB005132.
- Schlumberger (2007), *geoVISION: Resistivity imaging for productive drilling*.
- Screaton, E. et al. (2009), Interactions between deformation and fluids in the frontal thrust region of the NanTroSEIZE transect offshore the Kii Peninsula, Japan: Results from IODP Expedition 316 Sites C0006 and C0007, *Geochemistry, Geophys. Geosystems*, 10(12), doi:10.1029/2009GC002713.
- Sloan, E. D., and C. Koh (2007), *Clathrate Hydrates of Natural Gases, Third Edition*, Chemical Industries, CRC Press.
- Spangenberg, E. (2001), Modeling of the influence of gas hydrate content on the electrical properties of porous sediments, *J. Geophys. Res. Solid Earth*, 106, 6535–6548.
- Sultan, N. (2007), Comment on “Excess pore pressure resulting from methane hydrate dissociation in marine sediments: A theoretical approach” by Wenyue Xu and Leonid N. Germanovich, *J. Geophys. Res. Solid Earth*, 112(2), 1–7, doi:10.1029/2006JB004527.
- Vanderbeek, B. P., and A. W. Rempel (2018), On the Importance of Advective Versus Diffusive Transport in Controlling the Distribution of Methane Hydrate in Heterogeneous Marine Sediments, , 1, doi:10.1029/2017JB015298.
- Waite, W. F. et al. (2009), Physical properties of hydrate-bearing sediments, *Rev. Geophys.*, 47(4), 1–38, doi:10.1029/2008RG000279.
- Wallace, L. M. et al. (2009), Characterizing the seismogenic zone of a major plate boundary subduction thrust: Hikurangi Margin, New Zealand, *Geochemistry, Geophys. Geosystems*, doi:10.1029/2009GC002610.

- Wallace, L. M., J. Beavan, S. Bannister, and C. Williams (2012), Simultaneous long-term and short-term slow slip events at the Hikurangi subduction margin , New Zealand : Implications for processes that control slow slip event occurrence , duration , and migration, *J. Geophys. Res. Solid Earth*, *117*, 1–18, doi:10.1029/2012JB009489.
- Wallace, L. M., S. C. Webb, Y. Ito, K. Mochizuki, R. Hino, S. Henrys, S. Y. Schwartz, and A. F. Sheehan (2016), Slow slip near the trench at the Hikurangi subduction zone, New Zealand, *Science* (80-.), *352*(6286), 1–5.
- Wallace, L. M., D. M. Saffer, P. M. Barnes, I. A. Pecher, K. E. Petronotis, A. LeVay, L.J., and the E. 372/375 S. Proceedings (2019), Expedition 372B/375 methods, , *372B/375*.
- Watson, S. J. et al. (2019), Focused fluid seepage related to variations in accretionary wedge structure, Hikurangi margin, New Zealand, *Geology*, *48*(1), 56–61, doi:10.1130/G46666.1.
- Weinberger, J. L., and K. M. Brown (2006), Fracture networks and hydrate distribution at Hydrate Ridge, Oregon, *Earth Planet. Sci. Lett.*, *245*(1–2), 123–136, doi:10.1016/j.epsl.2006.03.012.
- Xu, W., and L. N. Germanovich (2006), Excess pore pressure resulting from methane hydrate dissociation in marine sediments: A theoretical approach, *J. Geophys. Res. Solid Earth*, *111*(1), 1–12, doi:10.1029/2004JB003600.
- Yun, T. S., F. M. Francisca, J. C. Santamarina, and C. Ruppel (2005), Compressional and shear wave velocities in uncemented sediment containing gas hydrate, *Geophys. Res. Lett.*, *32*(10), 1–5, doi:10.1029/2005GL022607.